Electron collisions with the H_2CN radical using the *R*-matrix method

Kedong Wang,* Yipeng An, Ju Meng, Yufang Liu, and Jinfeng Sun
College of Physics and Electronic Engineering, Henan Normal University, Xinxiang 453007, China
(Received 25 January 2014; published 28 February 2014)

Ab initio scattering calculations for low-energy electron collisions with an open-shell molecule H_2CN have been carried out using the *R*-matrix method. The elastic integral, differential, and momentum transfer cross sections and the excitation cross sections from the ground state to the three low-lying electron excited states are presented in the energy region of 0–10 eV. The results of the static exchange, correlated 1-state and 14-state close-coupling approximations are investigated to identify the low-lying resonant states of the anions formed due to electron capture by the radical. Four shape resonances and three core-excited shape resonances have been detected in the 14-state model. The Born-closure approximation is applied for the elastic and dipole-allowed transitions to account for the $l > 4$ partial waves excluded from the *R*-matrix calculations.

DOI: 10.1103/PhysRevA.89.022711 PACS number(s): 34.80.Bm, 34.80.Gs

I. INTRODUCTION

The methylene amidogene radical (H_2CN), discovered in 1962 by Cochran *et al*. [1], is an important intermediate in the combustion of nitramine propellants [2] and plays a role in extraterrestrial atmospheres [2–4]. It was also detected in interstellar clouds [5]. Because of its special importance in these aspects, H_2CN has been the subject of many experimental and theoretical studies.

The absorption spectra of H_2CN have been measured by many groups [6–9], and a number of diffuse bands were observed at 4.31–4.44 eV. Complementary to these experimental studies have been a number of theoretical investigations of the electronic state of H_2CN. The ground electronic state of H_2CN is $X\,^2B_2$, and the structure is planar with C_{2v} symmetry [6]. The vertical excitation energies from $X\,^2B_2$ to the first four excited states $1\,^2B_1$, $1\,^2A_1$, $2\,^2B_1$, and $1\,^4B_2$ were reported by Adams *et al*. [10] at the complete active space multiconfiguration plus singles and doubles configuration interaction (MCSCF/SDCI) level as 4.40, 4.46, 5.16, and 5.32 eV, respectively. Brinkmann *et al*. [11] also predicted that vertical excitation energies from $X\,^2B_2$ to the first three excited states $1\,^2B_1$, $2\,^2B_1$, and $1\,^2A_1$ at the equation-of-motion coupled cluster singles doubles (EOM-CCSD) level with cc-pVQZ basis set as 4.13, 4.34, and 4.73 eV, respectively. So [12] proposed that the lowest adiabatically excited state has a nonplanar equilibrium geometry, with $2A'$ symmetry. It has been shown that the lowest $^2A_1$ state was calculated to be planar, whereas the $2\,^2B_1$ state was predicted to relax to a nonplanar equilibrium structure. Both Bernad *et al*. [13] and Nizamov *et al*. [14] assigned their observed absorption bands to a vibronically allowed $1\,^2B_1 \leftarrow X\,^2B_2$ transition. Subsequently, Eisfeld and co-workers [15–17] carried out a series of theoretical and experimental studies of the electronic states of H_2CN and assigned the observed electronic transition as the dipole-allowed $1\,^2A_1 \leftarrow X\,^2B_2$ transition.

The experimental data on the basic properties for the ground-state H_2CN, such as electron affinity (EA) and rotational constants are also available. Cowles *et al*. [18] measured the ultraviolet photoelectron spectra of H_2CN^- and deduced the adiabatic electron affinity of the H_2CN molecule to be 0.511 ± 0.008 eV. Eisfeld [16] calculated the adiabatic electron affinity of 0.5152 eV calculated with zero-point energy correction. The rotational constants of H_2CN were determined to be 9.4844, 1.3062, and 1.1423 cm^{-1} by the microwave spectroscopy [19].

To the best of our knowledge, there have been no reports on the low-energy electron collision with H_2CN. In the low-energy electron collisions with molecules, not only the electron transitions including the spin-permitted and spin-forbidden promotions can be observed, but also the coupling mechanism between the electron-molecule resonant states formed in the collisions can be investigated. In the present work, we use the UK molecular *R*-matrix code [20–22] to study the low-energy electron scattering of H_2CN in the fixed-nuclei approximation. This method can provide a good description of the electron correlations in several excited states of the molecule, and has been demonstrated in a series of studies on polyatomic molecules [23]. Our interest lies in the low-energy region (0–10 eV) where the *R*-matrix method works best. The incoming electron can occupy one of the unoccupied molecular orbitals or can excite any of the occupied molecular orbitals as it falls into another one. These electron-molecule resonant states are usually short lived and decay into energetically open channels, e.g., dissociation to a negative ion and a neutral fragment. Below the threshold of the first vibrational channel, the energy loss is due to rotational excitations, which is very important for polar molecules where the cross section becomes enormous. The electron-scattering calculations are performed at the static-exchange (SE) and close-coupling (CC) approximations (one state and many states).

II. METHOD

A. Theory

The *R*-matrix method has been described in detail elsewhere [24]. In a fixed-nuclei *R*-matrix approach, the coordinate space is divided into an inner region and an outer region. The origin of the coordinate system was defined at the center of mass of the molecule. In the inner region, the scattering electron is indistinguishable from the electrons of the target and the electron correlation and exchange are

*Corresponding author: wangkd@htu.cn

 ©2014 American Physical Society

strong. In the outer region, it is assumed that the scattering electron is distinct. This electron therefore moves in a local potential arising from its long-range interaction with the target. The electron exchange and correlation effects between the scattering electron and target electrons are neglected.

In the inner region, the wave function of the scattering system consisting of the target plus scattering electron is written using the configuration interaction (CI) expression

$$\Psi_k^{N+1} = A\sum_{ij} a_{ijk}\Phi_i^N(x_1,\ldots,x_N)u_{ij}(x_{N+1}) + \sum_i b_{ik}\chi_i^{N+1}(x_1,\ldots,x_{N+1}), \quad (1)$$

where A is an antisymmetrization operator, x_N is the spatial and spin coordinate of the Nth electron, ϕ_i^N represents the ith state of the N-electron target, μ_{ij} is a continuum-orbital spin coupled with the scattering electron, and k refers to a particular R-matrix basis function. Coefficients a_{ijk} and b_{ik} are variational parameters determined as a result of the matrix diagonalization. The sum in the second term of Eq. (1) represents the short-range correlation and polarization effects, running over all configurations ${\chi_i}^{N+1}$ that are known as L^2 functions. These are also important for relaxing the orthogonality imposed between the target and continuum orbitals.

In the present calculation the target molecular obital space is divided into core (inactive), valence (active), and virtual orbitals. These target molecular obritals are supplemented with a set of continuum orbitals, centered on the center of mass of the molecule. In the polyatomic R-matrix calculations, the regions are separated by a spherical boundary of radius $\sim 12a_0$. This sphere is large enough to enclose the whole charge density of N electrons in the target states of interest (and L^2 functions). The continuum orbitals are Gaussian-type orbitals (GTOs). First, a Schmidt orthogonalization procedure is used to orthogonalize target and continuum molecular orbitals (MOs), then Löwdin symmetric orthogonalization is used to orthogonalize the continuum orbitals among themselves and remove linearly dependent functions [21,25].

B. Target model

H_2CN, whose structure belongs to the C_{2v} point group, is an open-shell system. The structural parameters with an angle of H-C-H=116.35°, two bonds of C-N=1.2478 Å and C-H=1.1009 Å are reported in the Computational Chemistry Comparison and Benchmark Database (CCCBDB) [26] and used in the present calculations. The restricted open-shell Hartree-Fock self-consistent field (SCF) wave function for ground-state H_2CN was obtained using the double ζ plus polarization Gaussian basis set [27], contracted as $(9s5p1d)/(4s2p1d)$ for both the C and N atoms, and $(4s1p)/(2s1p)$ for the H atom. The SCF energy at the ground state using this basis set is −93.094 060 a.u. and the electronic configuration is $1a_1{}^2 2a_1{}^2 3a_1{}^2 4a_1{}^2 1b_2{}^2 5a_1{}^2 1b_1{}^2 2b_2{}^1$. The CI model is employed to improve the calculations of the ground and excited states. In the CI model eight frozen electrons were distributed in the $1a_1$-$4a_1$ configuration and the remaining seven electrons are allowed to move freely in 11 molecular orbitals $5a_1$-$9a_1$, $1b_1$-$3b_1$, and $1b_2$-$3b_2$. The CI energy of the ground state is lowered to −93.480 788 a.u. To provide additional information on the charge distribution in the H_2CN molecule, we have also calculated the dipole and quadrupole moments. The dipole moment of μ value at the ground state is predicted to be 2.476 D, which is in good agreement with the value 2.54 D reported by Cowles [18]. The difference in the two is due to the inclusion of correlation effects lowering the value of the dipole moment in the CI model. The components of the quadrupole moments Q_{20} and Q_{22} are 0.381 975 and 1.361 387 a.u., respectively.

No R-matrix poles in the $^1A_1$ scattering symmetry with energies below that of the ground-state $X\,^2B_2$ are found, which indicates that there is no bound state of the anion H_2CN^-. However, this bound state can be formed in the experiment with electron EA of 0.511 eV [18]. The existence of a bound negative ion may seriously influence the cross sections at the corresponding symmetry $^1A_1$ for the bound-state H_2CN^-. In this work, the SCF calculations for the ground-state ($^1A_1$) H_2CN^- at the H_2CN equilibrium geometry have been performed. The energy of the highest occupied MO $^1A_1$ is 0.49 eV. The vertical EA of 0.49 eV can be simply estimated within Koopman's theorem, which is close to the experimental result [18]. Furthermore, using the SCF wave functions of H_2CN^-, the CI calculations predict a pole of $^1A_1$ symmetry, which is 0.43 eV lower than the ground-state energy of H_2CN. Therefore, this $^1A_1$-state anion H_2CN^- is a bound state. The modified SCF orbitals for $^1A_1$ symmetry are only used for the calculations of the elastic cross section, while the SCF orbitals of H_2CN are used for the other calculations.

Table I lists the dominant configurations, the number of configuration-state functions, and the vertical excitation energies of the target states. Our calculated vertical excited energies for the four low-lying excited states are in good agreement with the MCSCF results of Adams *et al.* [10]. The first vertical excited energy predicted by us agrees well with the experimental value [13]. For the 1^2A_1 state our value is higher by 0.66 eV than the experimental value [13]. For the higher excited state, there is no experimental data available. The difference between our results and multireference configuration interaction (MRCI) work [15] is due to the different basis set, the active space, and the correlation effects used.

C. Scattering model

In the present work, 14 target states are used to describe the electron plus target system. Of these 14 target states 2 states are in $^2A_2$ symmetry, and each 3 is in $^2B_2$, $^2A_1$, and $^2B_1$, and each 1 is in $^4B_2$, $^4A_2$, and $^4A_1$ symmetries, respectively. The scattering calculations are carried out for singlet and triplet states with A_1, B_1, B_2, and A_2 symmetries. The continuum orbitals up to g partial waves are orthogonalized to the target orbitals based on the mixture of Schmidt and Löwdin symmetric orthogonalization [28] and represented by GTOs centered at the molecular center of gravity [29]. In order to obtain the good balance between the representation of the target wave function and the scattering wave function, eight electrons (seven valance electrons plus one scattering electron) are allowed to move freely among $5a_1$, $6a_1$, $7a_1$, $8a_1$, $9a_1$, $1b_1$, $2b_1$, $3b_1$, $1b_2$, $2b_2$, and $3b_2$ molecular orbitals.

TABLE I. Predominant configuration, transition moment (in a.u.), the number of configuration-state functions (N), and the vertical excitation energies (in eV) for the target states of H_2CN.

State	Dominant configuration	Transition moment	N	Vertical excited energy				
				This work	MCSCF[a]	CCSD[b]	MRCI[c]	Expt.
$X\,^2B_2$	$\text{—}1b_2^2 5a_1^2 1b_1^2 2b_2^1$	0.9739[d]	7260	0	0	0	0	0
$1\,^2B_1$	$\text{—}1b_2^2 5a_1^2 1b_1^1 2b_2^2$		7260	4.37	4.40	4.13	3.94	4.35[e],
$1\,^2A_1$	$\text{—}1b_2^2 5a_1^1 1b_1^2 2b_2^2$	−0.2297	7364	5.08	4.46	4.34	4.34	4.43[e],4.31–4.44[f]
$2\,^2B_1$	$\text{—}1b_2^2 5a_1^2 2b_2^2 2b_1^1$		7260	5.28	5.16	4.73	4.35	
$1\,^4B_2$	$\text{—}1b_2^2 5a_1^2 1b_1^1 2b_2^1 2b_1^1$		5072	5.31	5.32			
$2\,^2B_2$	$\text{—}1b_2^2 5a_1^2 1b_1^2 3b_2^1$	−0.0493	7260	6.59				
$1\,^4A_2$	$\text{—}1b_2^2 5a_1^2 1b_1^1 2b_2^1 6a_1^1$		5176	7.30				
$1\,^2A_2$	$\text{—}1b_2^2 5a_1^2 1b_1^1 2b_2^1 6a_1^1$	−0.2783	7156	8.40				
$3\,^2B_2$	$\text{—}1b_2^2 5a_1^2 3b_2^1 2b_1^2$	0.0505	7260	9.18				
$1\,^4A_1$			5008	9.78				
$2\,^2A_2$		0.2077	7156	10.14				
$2\,^2A_1$		0.4318	7364	10.25				
$3\,^2A_1$		−0.9972	7364	10.69				
$3\,^2B_1$			7260	11.19				

[a]From Ref. [11] (MCSCF/SDCI).
[b]From Ref. [12] (EOM-CCSD/cc-pVQZ).
[c]From Ref. [16] (MRCI/aug-cc-pVTZ).
[d]Static dipole moment for the ground state.
[e]From Ref. [14].
[f]From Ref. [18].

III. RESULTS

A. Elastic cross sections

The elastic cross sections of electron collision with H_2CN for $^1A_1$ symmetry in three different models, viz., SE, one state, and many-states CI models are shown in Fig. 1. As mentioned above, the first $^1A_1$ state of the anion H_2CN^- is a bound state. The SE model predicts a broad peak at about 9.00 eV for $^1A_1$ symmetry. This peak becomes narrow at almost the same place in the correlated 1-state model. However, the peak vanishes in the many-states model, indicating the bound-state nature of this state.

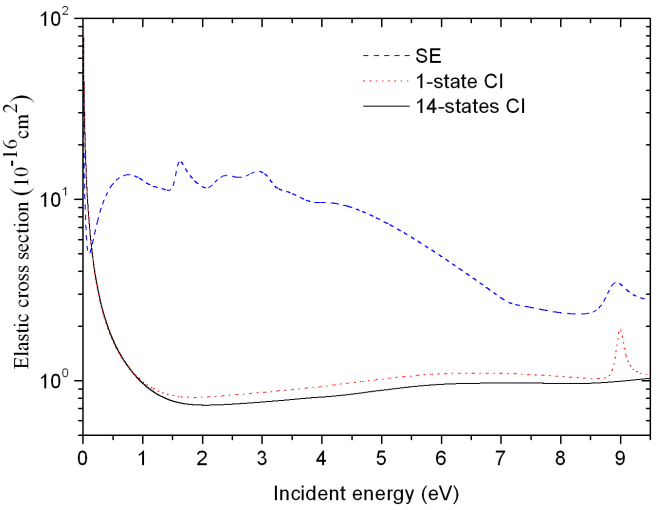

FIG. 1. (Color online) Elastic cross sections of the electron impact on the H_2CN molecule for the $^1A_1$ scattering symmetry state. Dashed line: SE; dotted line: 1-state CI; solid line: 14-states CI.

Figure 2 shows the four component cross sections (both singlet and triplet), together with the summed elastic integral and Born-corrected cross sections. The maximum contributions to the singlet and triplet components are that of the $^1B_2$ and $^3B_2$ symmetries, respectively. There is a peak around 3.17 eV with a width of 0.013 eV in $^1A_2$ scattering symmetry. The peak around 2.48 eV with a width of 0.013 eV is also detected in $^3A_2$ scattering symmetry. Due to the presence of the long-range dipole interaction, the elastic cross sections are formally divergent in the fixed-nuclei approximation as the differential cross section (DCS) is singular in the forward direction. To obtain converged cross sections, the effect of rotation must be included along with a very large number of partial waves. The effects of partial waves with $l > 4$ were included using a Born correction via a closure approach [30,31]. As shown in Fig. 2(c), the contribution of the Born correction is larger than that of the summed elastic integral cross sections at the present energy regions 0–10.0 eV. This is because H_2CN has a large static dipole moment and the Born correction for the rotational $(0 \rightarrow 1)$ component is significant.

The scattering resonances in a multichannel calculation are characterized not only by the mere structures in the cross sections but also, more importantly, by the increase of the eigenphase sum for about π radians in a (generally) narrow energy range. In most cases, the resonance parameters can be extracted from eigenphase sums matched to a Breit-Wigner profile [32]

$$\delta(E) = \delta_0(E) - \tan^{-1}\left(\frac{\Gamma/2}{E_r - E}\right), \tag{2}$$

where E_r is the resonance position, Γ is the width, and $\delta_0(E)$ is the background phase near the resonance. When the

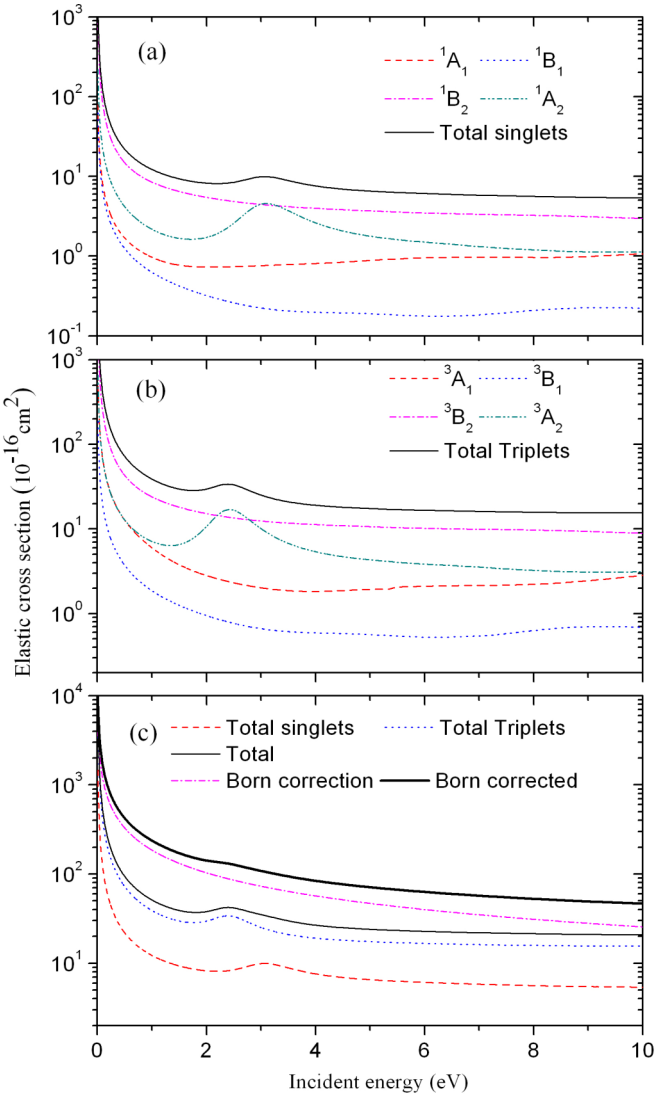

FIG. 2. (Color online) Elastic cross sections in the energy range of 0–10 eV. (a) Dashed line: $^1A_1$; dotted line: $^1B_1$; dashed-dotted line: $^1B_2$; dashed-double-dotted line: $^1A_2$; solid line: total singlets. (b) Dashed line: $^3A_1$; dotted line: $^3B_1$; dashed-dotted line: $^3B_2$; dashed-double-dotted line: $^3A_2$; solid line: total triplets. (c) Dashed line: total singlets; dotted line: total triplets; solid line: total (singlets + triplets); dashed-dotted line: Born correction; thick solid line: Born corrected.

background varies slowly over the resonance profile, Γ can be determined from the relation [33]

$$\Gamma = 2/\delta'(E_r). \tag{3}$$

In general, the point of maximum gradient $\delta'(E)$ serves as the definition for the position of the resonance, and the width can be determined using Eq. (3). All resonances revealed in the present calculations are presented in Table II, together with the values of their resonance parameters. Both the peak at 2.48 eV at the $^3A_2$ symmetry and the peak at 3.17 eV at $^1A_2$ symmetry are shape resonances with the same configuration $(X\,^2B_2)2b_1^1$. These two shape resonances are with the ground-state $X\,^2B_2$ as their parent state.

B. Inelastic cross sections

The electronic excitation cross section from the ground-state $X\,^2B_2$ to the first excited state $1\,^2B_1$ is depicted in Fig. 3. This is a dipole forbidden but vibronically allowed transition. A shape peak appears in the cross section for $^3A_1$ symmetry at 5.40 eV with a width of 0.014 eV, which is due to a resonance formed as a result of the $3b_2$ molecular orbital getting attached to the $X\,^2B_2$ basis state. This is termed as a shape resonance. We notice a peak in the $^3B_1$ symmetry at 7.03 eV with a width of 0.013 eV which is associated with configuration $-1b_2^2 5a_1^2 1b_1^2 2b_2^1 1a_2^1$. It is also a shape resonance which can decay to the parent state $X\,^2B_2$. The peak at 9.20 eV in $^1B_2$ symmetry with a width of 0.023 eV is a core-excited resonance. The parent state of this core-excited resonance is $3\,^2B_2$ with the configuration $-1b_2^2 5a_1^2 3b_2^1 2b_1^2 6a_1^1$. The sharp peak at 9.23 eV is related to a core-excited resonance $^3B_2$ with a width of 0.014 eV and a configuration $-1b_2^2 5a_1^2 3b_2^1 2b_1^2 6a_1^1$. It can decay to its parent state $3\,^2B_2$ if the electron of $6a_1$ is detached.

Figure 4 depicts the $X\,^2B_2 \rightarrow 1\,^2A_1$ excitation cross section which includes four C_{2v} symmetry components (both singlet and triplet), together with their sum. This transition is optically allowed, and the cross section for this transition has been Born corrected [30,31]. As shown in the figure, the Born correction cross section increases as the incident electron increases. The contribution of the $^3A_1$ symmetry is larger than that of the other seven symmetries. The sharp peak in the $^3A_1$ symmetry at 5.40 eV and the broad peak in the $^3B_1$ symmetry at 7.03 eV have been detected in the $X\,^2B_2 \rightarrow 1\,^2B_1$ transition. Both sharp peaks around 9.2 eV in the $^1B_2$ symmetry and the $^3B_2$ symmetry are also detected in the $X\,^2B_2 \rightarrow 1\,^2B_1$ transition. An additional broad peak at 8.57 eV is observed in Fig. 4, which is due to $^1B_1$ symmetry scattering. This $^1B_1$ symmetry resonance is further proven to be a core-excited shape resonant state with a width of 0.013 eV, and its configuration is $1b_2^2 5a_1^2 1b_1^1 2b_2^2 6a_1^1$ and can decay into the parent state $X\,^2A_2$ after the electron detachment from the $6a_1$ molecule orbital.

In Fig. 5, we have shown the excitation cross sections of the $X\,^2B_2$ to $2\,^2B_1$ transition. This is also a dipole-forbidden but vibronically allowed transition. The singlet and triplet components give similar contributions to the cross sections for this transition in the considered energy range. The peaks in $^3A_1$ symmetry at 5.40 eV, in $^3B_1$ symmetry at 7.03 eV, in $^1B_2$ symmetry at 9.20 eV, and in $^3B_2$ symmetry at 9.23 eV have been discussed before.

C. Differential cross section

The calculation of the DCSs provides a stronger test for any theoretical model. The DCS for a general polyatomic molecule is given by

$$\frac{d\sigma}{d\Omega} = \sum_L A_L P_L(\cos\,\theta), \tag{4}$$

where P_L is a Legendre function. The A_L coefficients have been discussed in detail before [34]. For a polar molecule this expansion over L converges slowly. The following closure formula is used to accelerate the convergence of DCS,

$$\frac{d\sigma}{d\Omega} = \frac{d\sigma^B}{d\Omega} + \sum_L \left(A_L - A_L^B\right) P_L(\cos\,\theta). \tag{5}$$

TABLE II. Resonant states of the electron-H_2CN scattering system.

State	Designation of resonance	Type	Resonance parameter (eV)		Parent state (eV)	
			Position	Width	State	Position
$^3A_2$	$-1b_2^2 5a_1^2 1b_1^2 2b_2^1 2b_1^1$	Shape	2.48	0.013	$X\,^2B_2$	0
$^1A_2$	$-1b_2^2 5a_1^2 1b_1^2 2b_2^1 2b_1^1$	Shape	3.17	0.013	$X\,^2B_2$	0
$^3A_1$	$-1b_2^2 5a_1^2 1b_1^2 2b_2^1 3b_2^1$	Shape	5.40	0.014	$X\,^2B_2$	0
$^3B_1$	$-1b_2^2 5a_1^2 1b_1^2 2b_2^1 1a_2^1$	Shape	7.03	0.013	$X\,^2B_2$	0
$^1B_1$	$-1b_2^2 5a_1^2 1b_1^1 2b_2^2 6a_1^1$	Core-excited	8.57	0.013	$1\,^2A_2$	8.40
$^1B_2$	$-1b_2^2 5a_1^2 3b_2^1 2b_1^2 6a_1^1$	Core-excited	9.20	0.023	$3\,^2B_2$	9.18
$^3B_2$	$-1b_2^2 5a_1^2 3b_2^1 2b_1^2 6a_1^1$	Core-excited	9.23	0.014	$3\,^2B_2$	9.18

The superscript B represents the relevant quantity which is calculated in the Born approximation with an electron-point dipole interaction. The convergence of the summation over L in Eq. (5) is now rapid because the contribution from the higher partial waves to the DCS is dominated by an electron-dipole interaction. The quantity $d\sigma^B/d\Omega$ for any initial rotor state $|J\tau\rangle$ is given by the sum over all the final rotor states $|J'\tau'\rangle$,

$$\frac{d\sigma^B}{d\Omega} = \sum_{J'\tau'} \frac{d\sigma^B}{d\Omega}(J\tau \to J'\tau'). \tag{6}$$

The expressions for the state-to-state rotationally inelastic DCS, $d\sigma^B/d\Omega(J\tau \to J'\tau')$, for a spherical top, a symmetric top, and asymmetric top molecules have been given by Sanna and Gianturco [35]. The calculated dipole moment (2.476 D) and rotational constants ($A = 9.5584\ \mathrm{cm}^{-1}$, $B = 1.2971\ \mathrm{cm}^{-1}$, and $C = 1.1421\ \mathrm{cm}^{-1}$) for H_2CN are used in the calculations of the DCSs ($J = 0 \to J' = 0,1,2,3, \ldots$).

Our calculated rotationally resolved DCSs for electron scattering by H_2CN at the incident energy of 2 eV for the singlet and triplet symmetries separately are shown in Figs. 6(a) and 6(b). Since H_2CN is a strong polar molecule, the $0 \to 1$ contribution is much bigger than the elastic $0 \to 0$ component except at the angles 20°–25°. Therefore the dominant feature of the state-resolved DCS is the dipole component $0 \to 1$. In general, the contribution of the higher J' decreases with the J' increases. We obtained almost convergent results when J' increases up to 5. The DCSs obtained by summarizing the rotational cross sections for ($J = 0 \to J' = 0$–5) at the selected energies of 0.5, 1, 2, 4, 6, and 8 eV are depicted in Fig. 7. Due to the dipolar nature of the target, the DCSs at all the energies show the sharp increases at the smaller scattering angles. The DCSs at 0.5, 1, and 2 eV show two minima at about 22° and 150°, respectively. When the incident energy increases to 4, 6, and 8 eV, one minimum of the DCS appears at about 72°. As yet there is no experimental or theoretical DCS available for comparison.

By using the POLYDCS program, the momentum transfer cross sections (MTCS) are calculated and presented in Fig. 8. The MTCS indicates the weights of backward-scattering and is useful in the study of electrons drifting through a molecular gas. We observe the MTCS decreases with the increasing energy. In contrast to the diverging nature of DCS in the

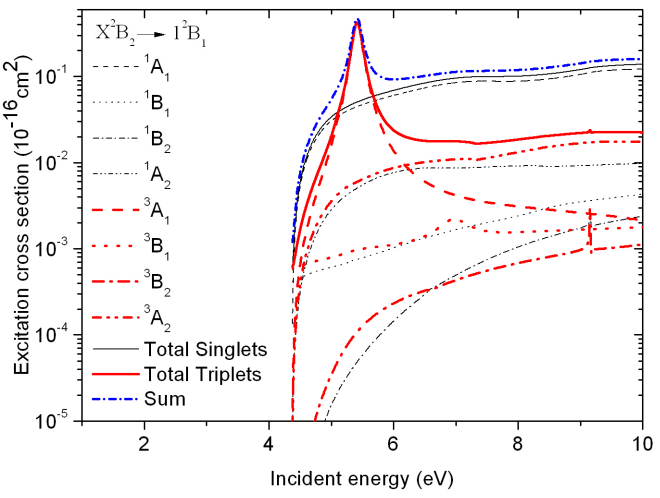

FIG. 3. (Color online) Electron-impact excitation cross sections from the ground-state $X\,^2B_2$ to the $1\,^2B_1$ state. Thin dashed line: $^1A_1$; thin dotted line: $^1B_1$; thin dashed-dotted line: $^1B_2$; thin dashed-double-dotted line: $^1A_2$; thin solid line: total singlets; thick dashed line: $^3A_1$; thick dotted line: $^3B_1$; thick dashed-dotted-line: $^3B_2$; thick dashed-double-dotted line: $^3A_2$; thick solid line: total triplets; thick and short-dashed-dotted line: sum.

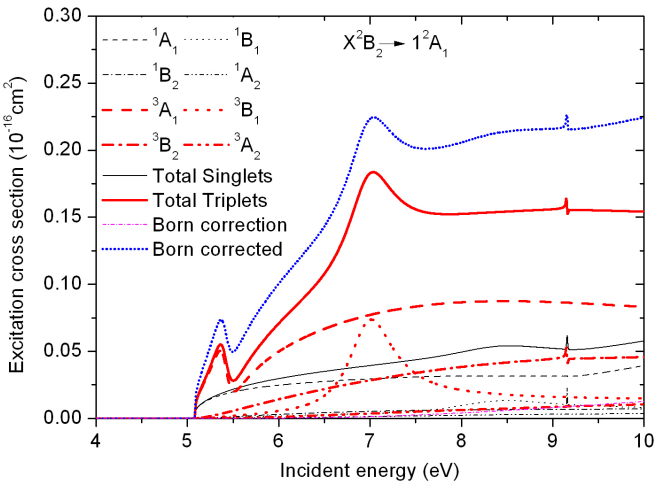

FIG. 4. (Color online) Electron-impact excitation cross sections from the ground-state $X\,^2B_2$ to the $1\,^2A_1$ state. Thin dashed line: $^1A_1$; thin dotted line: $^1B_1$; thin dashed-dotted line: $^1B_2$; thin dashed-double-dotted line: $^1A_2$; thin solid line: total singlets; thick dashed line: $^3A_1$; thick dotted line: $^3B_1$; thick dashed-dotted line: $^3B_2$; thick dashed-double-dotted line: $^3A_2$; thick solid line: total triplets; thin and short-dashed-dotted line: Born correction; thick and short-dotted line: Born corrected.

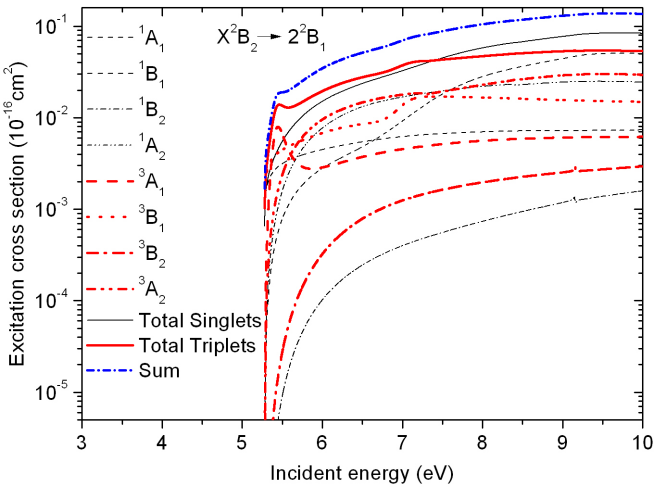

FIG. 5. (Color online) Electron-impact excitation cross sections from the ground-state $X\,^2B_2$ to the $2\,^2B_1$ state. Thin dashed line: $^1A_1$; thin dotted line: $^1B_1$; thin dashed-dotted line: $^1B_2$; thin dashed-double-dotted line: $^1A_2$; thin solid line: total singlets; thick dashed line: $^3A_1$; thick dotted line: $^3B_1$; thick dashed-dotted-line: $^3B_2$; thick dashed-double-dotted line: $^3A_2$; thick solid line: total triplets; thick and short-dashed dotted line: sum.

forward direction (at the large scattering angles), MTCS show no singularity due to the multiplicative factor $(1-\cos\theta)$, where θ is the scattering angle. It is obvious that three shape resonances at 2.48, 5.40, and 7.03 eV and a core-excited resonance

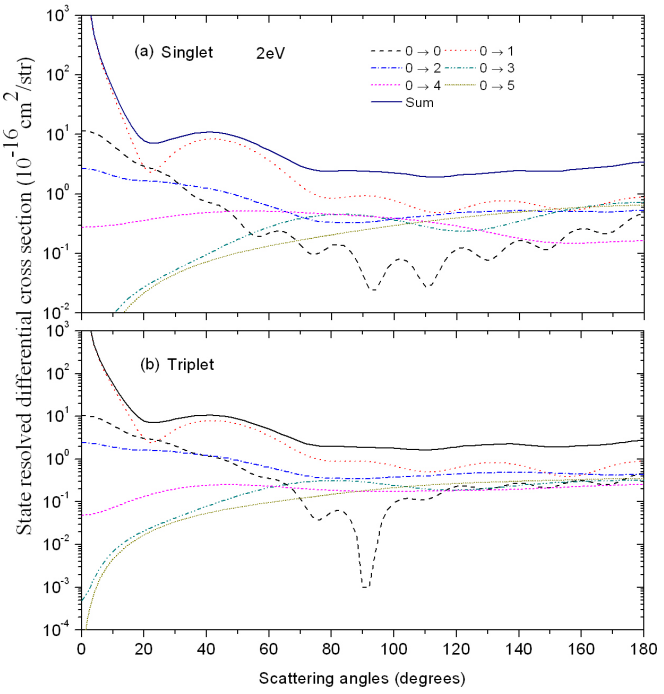

FIG. 6. (Color online) Electron impact R matrix rotationally resolved state-to-state ($J \rightarrow J'$) differential cross sections of H_2CN at 2 eV. Dashed curve: $J = 0 \rightarrow J' = 0$; dotted curve: $J = 0 \rightarrow J' = 1$; dash-dotted curve: $J = 0 \rightarrow J' = 2$; dash-double-dotted curve: $J = 0 \rightarrow J' = 3$; short-dashed curve: $J = 0 \rightarrow J' = 4$; short dotted curve: $J = 0 \rightarrow J' = 5$; solid curve: summed. (a) Singlets. (b) Triplets.

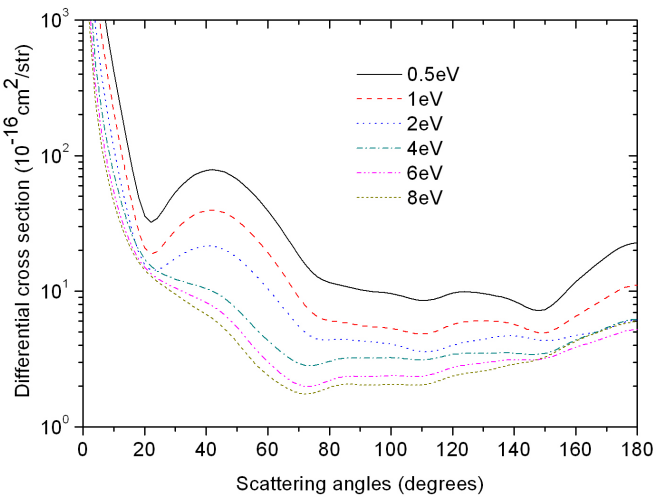

FIG. 7. (Color online) Differential cross section at different energies 0.5, 1, 2, 4, 6, and 8 eV. Solid curve: 0.5 eV; dashed curve: 1 eV; dotted curve: 2 eV; dash-dotted curve: 4 eV; dash-double-dotted curve: 6 eV; short-dashed curve: 8 eV.

at 8.57 eV are responsible for the peaks observed at around 2.45, 5.42, 7.02, and 8.55 eV in the MTCS, respectively.

IV. CONCLUSION

The elastic and excitation inelastic cross sections of the low-energy electron collision with the H_2CN molecule are calculated using the R-matrix method. For the low-lying excited states of the target, our calculated vertical excited energies are in good agreement with the MCSCF results [10]. The electron scattering calculations show four shape resonant states $^3A_2$ (2.48 eV), $^1A_2$ (3.17 eV), $^3A_1$ (5.40 eV), and $^3B_1$ (7.03 eV), and three core-excited resonant states $^1B_1$ (8.57 eV), $^1B_2$ (9.20 eV), and $^3B_2$ (9.23 eV). Moreover, the elastic and rotationally inelastic differential cross sections are also calculated in which K-matrix elements are required and obtained within the 14-state CI model. The DCSs show sharp increases as the scattering angle approaches zero due to the

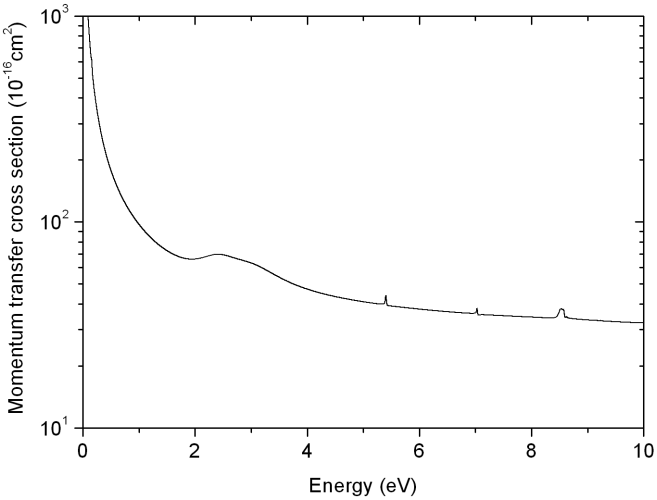

FIG. 8. Momentum transfer cross section for an energy range of 0.01–10.00 eV.

dipolar nature of the target molecule. The dipole component ($J = 0 \rightarrow J' = 1$) is also much larger than the elastic component ($J = 0 \rightarrow J' = 0$) in the total DCSs. As far as we know, there are no experimental or theoretical DCSs available for comparison. Furthermore, three shape resonances at 2.48, 5.40, and 7.03 eV and a core-excited resonance at 8.57 eV are also observed in the MTCS for H_2CN calculated in the present work.

ACKNOWLEDGMENTS

This work is partially supported by the Foundation of Henan Educational Committee (Grants No. 2011A140015 and No. 12A140006), National Development Fund of Henan Normal University (Grant No. 2012PL02), and NSFC (Grants No. 11304084 and No. U1304109). Dr. S. B. Zhang and Dr. Y. F. Wang are acknowledged for their kind help on calculations.

[1] E. L. Cochran, F. J. Adrian, and V. A. Bowers, J. Chem. Phys. **36**, 1938 (1962).
[2] G. Marston and L. J. Stief, Res. Chem. Intermed. **12**, 161 (1989).
[3] G. Marston, F. L. Nesbitt, and L. J. Stief, J. Chem. Phys. **91**, 3483 (1989).
[4] F. L. Nesbitt, G. Marston, L. J. Stief, M. A. Wickramaaratchi, W. Tao, and R. B. Klemm, J. Phys. Chem. **95**, 7613 (1991).
[5] M. Ohishi, D. McGonagle, W. M. Irvine, S. Yamamoto, and S. Saito, Astrophys. J. **427**, L51 (1994).
[6] J. F. Ogilvie and D. G. Horne, J. Chem. Phys. **48**, 2248 (1968).
[7] D. G. Horne and R. G. W. Norrish, Proc. R. Soc. Lond. A **315**, 287 (1970).
[8] D. G. Horne and R. G. W. Norrish, Proc. R. Soc. Lond. A **315**, 301 (1970).
[9] M. E. Jacox, J. Phys. Chem. **91**, 6595 (1987).
[10] G. F. Adams, D. R. Yarkony, R. J. Bartlett, and G. D. Purvis, Int. J. Quantum Chem. **23**, 437 (1983).
[11] N. R. Brinkmann, S. S. Wesolowski, and H. F. Schaefer III, J. Chem. Phys. **114**, 3055 (2001).
[12] S. P. So, Chem. Phys. Lett. **82**, 370 (1981).
[13] E. J. Bernard, B. R. Strazisar, and H. F. Davis, Chem. Phys. Lett. **313**, 461 (1999).
[14] B. Nizamov and P. J. Dagdigian, J. Phys. Chem. A **107**, 2256 (2003).
[15] W. Eisfeld, J. Chem. Phys. **120**, 6056 (2004).
[16] W. Eisfeld, Phys. Chem. Chem. Phys. **7**, 832 (2005).
[17] A. Teslja, P. J. Dagdigian, M. Banck, and W. Eisfeld, J. Phys. Chem. A **110**, 7826 (2006).
[18] D. C. Cowles, M. J. Travers, J. L. Frueh, and G. B. Ellison, J. Chem. Phys. **94**, 3517 (1991).
[19] S. Yamamoto and S. Saito, J. Chem. Phys. **96**, 4157 (1992).
[20] L. A. Morgan, C. J. Gillan, J. Tennyson, and X. Chen, J. Phys. B **30**, 4087 (1997).
[21] L. A. Morgan, J. Tennyson, and C. J. Gillan, Comput. Phys. Commun. **114**, 120 (1998).
[22] J. M. Carr, P. G. Galiatsatos, J. D. Gorfinkiel, A. G. Harvey, M. A. Lysaght, D. Madden, Z. Masin, M. Plummer, J. Tennyson, and H. N. Varambhia, Eur. Phys. J. D **66**, 58 (2012); J. Tennyson, Phys. Rep. **491**, 29 (2010).
[23] A. Dora, J. Tennyson, L. Bryjko, and T. Van Mourik, J. Chem. Phys. **130**, 164307 (2009); A. Dora, L. A. Bryjko, T. V. Mourik, and J. Tennyson, *ibid.* **136**, 024324 (2012); A. Bharadvaja, S. R. Kaur, and K. L. Baluja, Phys. Rev. A **87**, 062703 (2013); Z. Mašín and J. D. Gorfinkiel, J. Chem. Phys. **137**, 204312 (2012); S. B. Zhang, J. G. Wang, R. K. Janev, and X. J. Chen, Phys. Rev. A **82**, 062711 (2010); Y. F. Wang and S. X. Tian, *ibid.* **85**, 012706 (2012).
[24] P. G. Burke, *R-Matrix Theory of Atomic Collisions: Application to Atomic, Molecular and Optical Processes* (Springer-Verlag, Berlin, 2011).
[25] B. M. Nestmann, K. Pfingst, and S. D. Peyerimhoff, J. Phys. B: At., Mol. Opt. Phys. **27**, 2297 (1994).
[26] NIST, Computational Chemistry Comparison and Benchmark Database, http://cccbdb.nist.gov
[27] T. H. Dunning and P. J. Hay, in *Methods of Electronic Structure Theory*, edited by H. F. Schaefer, Vol. 2 (Plenum, New York, 1977).
[28] P. G. Burke and C. J. Noble, in *Swarm Studies and Inelastic Electron Molecule Collisions*, edited by L. C. Pritcharda, V. McKoy, A. Chutjian, and S. Trajmar (Springer, New York, 1987), p. 265.
[29] A. Faure, J. D. Gorfinkiel, L. A. Morgan, and J. Tennyson, Comput. Phys. Commun. **144**, 224 (2002).
[30] S. Kaur, K. L. Baluja, and J. Tennyson, Phys. Rev. A **77**, 032718 (2008).
[31] S. Kaur and K. L. Baluja, Phys. Rev. A **80**, 042701 (2009).
[32] J. Tennyson and C. J. Noble, Comput. Phys. Commun. **33**, 421 (1984).
[33] H. Friedrich, in *Theoretical Atomic Physics*, 3rd ed. (Springer, Berlin, 2006), p. 47.
[34] F. A. Gianturco and A. Jain, Phys. Rep. **143**, 347 (1986).
[35] N. Sanna and F. A. Gianturco, Comput. Phys. Commun. **114**, 142 (1998).